Technical University of Denmark

46320: Loads, Aerodynamics and Control of Wind Turbines

Individual Assignment

Nicola Quaia s232439

December 15, 2024

Introduction

In this report, a new version of the DTU 10 MW blade is proposed, building on the experience from the redesign done within Group 1. The new design has the same goal, which is to change the wind class from 1A to 3B, and should adhere to the same design criteria: increase the AEP while maintaining similar or lower design loads.
Hence, the following three blades will be analyzed: the original DTU 10 MW blade, referred to as 'DTU'; the redesign done in Group 1, referred to as 'redesign'; and the final new version, referred to as 'remodel', which is designed to address the issues with Group 1's blade.
In general, the redesigned blade had a reasonable shape but an inefficient control strategy, resulting in a lower Annual Energy Production (AEP) (- 1.19%). Additionally, a resonance phenomenon occurs at around 7 m/s, increasing the design loads. Therefore, the remodel will implement the following changes:

1. **shorter blade: - 1%** - to reduce the inertial moment, hence the design loads. The change is marginal not to compromise the power production
2. **larger chord: + 0.5%** - to increase the production. Small change not to increase the loads too much
3. **reduced safety margin when designing lift coefficient** - more aggressive aerodynamic design, to increase the production
4. **increased rotor speed** - to reduce torque after rated
5. **minimum rotor speed** - to avoid resonance problems
6. **peak shaving** - to reduce loads near rated
7. **lower cut-in speed** - as the new wind class shifts the wind probability towards smaller wind speeds, reducing the cut-in speed should increase the AEP.

Hence, a complete redesign of the blade is performed: first, the new shape is defined with a Pyton script, and tested with HAWC2S program to evaluate the operational point in terms of C_P and TSR. Then, the optimal operational data are computed for the rigid and flex blade, again with HAWC2S, and a modal analysis is performed on them using HAWCStab2. From here, the control settings can be tuned with HAWC2s and HAWC2, and finally, the design loads are evaluated with HAWC2 and the new AEP is computed.

1 Blade design

1.1 General parameters: R and V_{rated}

Table 1: IEC 61400-1:2019 standard, reporting only the information relative to this analysis. Note that V_{ave} is the annual average wind speed and I_{ref} is the reference value of the turbulence intensity.

Wind turbine class		**I**	**II**	**III**
V_{ave}	m/s	10	8.5	7.5
A+	I_{ref} (-)	0.18		
A	I_{ref} (-)	0.16		
B	I_{ref} (-)	0.14		
C	I_{ref} (-)	0.12		

The first step is to compute analytically the ideal new diameter size and reference wind speed to allow to change wind and turbulent class, based on the equations A and B given in Lecture 3 [2]. Combining the equations one can obtain Equation 1. As the original DTU 10 MW is developed for turbulent class A, the value of I_X is 0.16, as taken from Table 1, while the remodelled turbine has a class B, so $I_Y = 0.14$.

$$\begin{aligned} C &= \left(\frac{1+2I_X}{1+2I_Y}\right)^{2/3} \\ V_Y &= C^{-6/5}\ V_X \\ R_Y &= C^{9/5}\ R_X \end{aligned} \tag{1}$$

As mentioned above, the new rotor size does not follow strictly these equations, but is it reduced by an additional 1%, and the new wind speed is computed accordingly. The final values are reported in Table 2. The choice of reducing the radius is done to decrease the loads. Decreasing too much the value will decrease also the performance, so a resonable percentual reduction was chosen.

Table 2: Radius size and reference wind speed for the DTU 10 MW, the redesing done within Group 1 and the final remodel

	R [m]	V_{rated} [m/s]
DTU	89.170	11.400
redesign	92.524	11.123
remodel	91.599	11.198

1.2 Define blade shape

Hence, the new absolute thickness is increased, by multiplying the original thickness by a scaling factor of R_Y/R_X. However, the value at the root is maintained at the original value, as the new design should fit in the existing DTU hub, and we assume that the housing of the blade remains untouched. A similar considerations will be done later for the chord, as its root value will be left constant to DTU value.

To define the blade shape, the lift coefficient C_l as a function of the angle of attack AoA must be maximized for every airfoil, which is thickness dependent. However, taking the maximum C_l could lead to stall issues, so the numerical maximum must be reduced by a safety margin, and the AoA that corresponds to this reduced value is taken as the design angle of attack. Previously, in the redesign, a value of 0.4 was used as a safety margin. To boost the lift coefficient, so in theory the production, this value is reduced to 0.3 in the remodel. Graphically, this is explained in Figure 1.

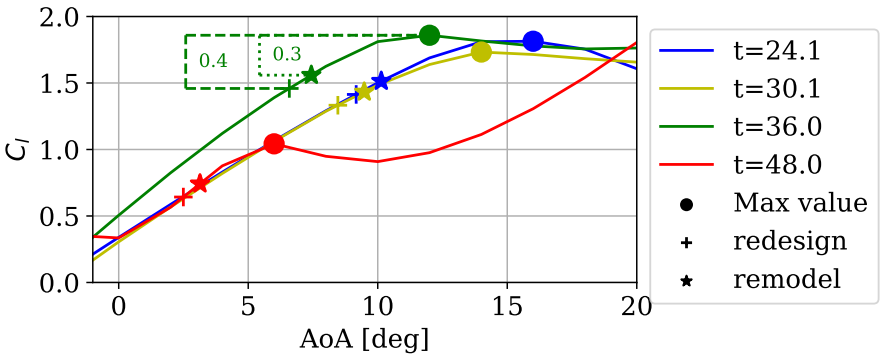

Figure 1: Lift coefficient as a function of the angle of attack for airfoils, defined by the relative thickness. Additionally, the maximum C_l point is plotted, as well as the value used in the redesign and in the remodel. The safety margin for the redesign and the remodel is displayed as well.

Hence, the found points are compared against the design functions evaluated using the `get_design_functions()` function in Figure 2. The different choice of safety margin allows for a different design function: now, function 1 is the closest to the computed values, and will be used in the following calculations.
Note that the use of a safety function, instead of taking the computed values, is done to avoid 'excessive' designs, that could lead to stall or other issues in the next steps of the design process. Hence, even though the new design function is 'more aggressive', it will unlikely lead to stall problems. It could, however, lead to excessive loads, but other design choices can be taken to avoid that.

Finally, the `single_point_design()` function can be used to define the shape of the blade in terms of chord, relative thickness and twist. Since the list of airfoil used is known, these data are sufficiently to define the blade shape. Additionally, the function performs a simplified BEM algorithm, and returns the induction factor a, the power coefficient C_P, and the thrust coefficient C_T, among others.

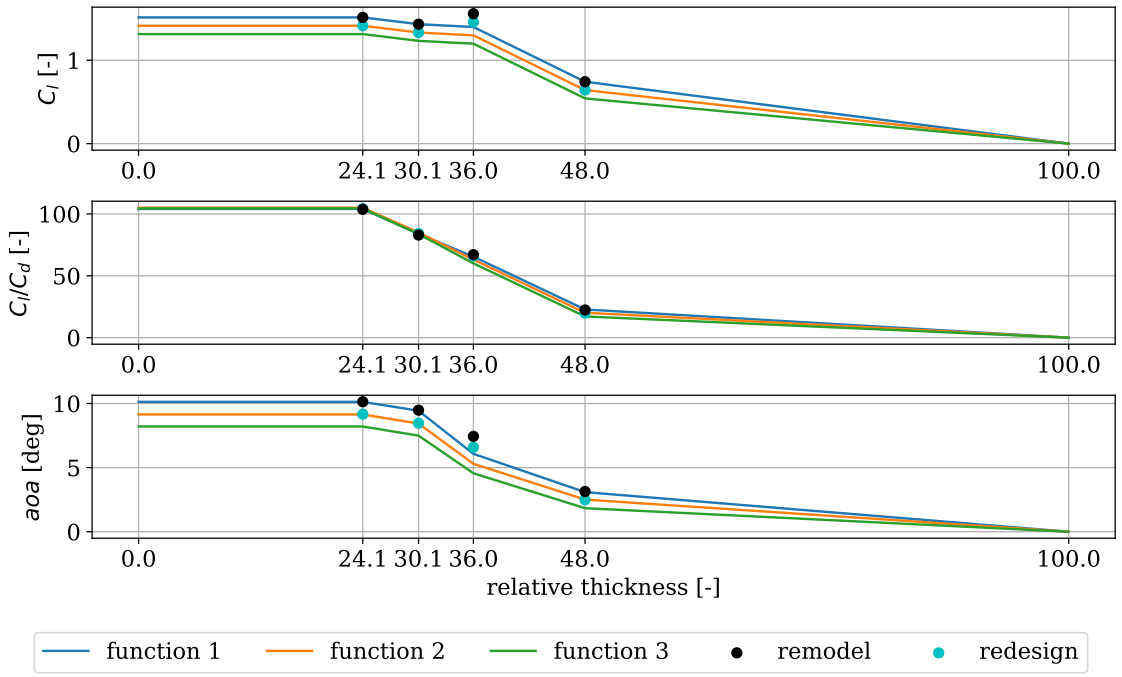

Figure 2: Found lift coefficient, lift over drag coefficient and angle of attack for the various airfoils for remodel and redesign, and design functions values.

First of all, the maximum chord is increased by 1%, changing the value from 6.3 to 6.363 m, to increase the production. As the section with the largest chord is near the root of the blade, the increased mass should not increase the loads too much, as the lever arm on the gravity moment is relatively small. Also, the change is so marginal that it will unlikely influence the next calculations.

So, the `single_point_design()` is evaluated for a range of TSR between 6 and 12. For each used TSR, a blade shape is defined, optimized for that input value. Then, the blade with the highest C_P is chosen as the optimal blade shape, and its parameters are used in the following steps. This procedure is portrayed in Figure 5.

The optimal shape is displayed in Figure 3 in terms of the chord, relative thickness and twist as a function of the rotor span. On the right (B), the percentual difference is given, to allow an easier understanding of the applied changes. It can be recalled that the relative thickness it computed as thickness divided by chord, so it is clear why the percentual change for chord and relative thickness looks symmetrical. The 'crazy' curve portrayed in the twist percentage difference is merely due to the DTU twist being close to 0, which makes the percentual difference increase rapidly. Moreover, the difference between the remodel and the redesign is very small: only around normalized span = 0.2 one can notice the new chord being larger, hence the relative thickness reducing.
As mentioned above, the problems of Group 1's blade were found mostly in choices done in the next stages of the design, not in the blade shape itself. Hence, obtaining a similar result for the remodel is good news, as it means that the steps done so far are correct.

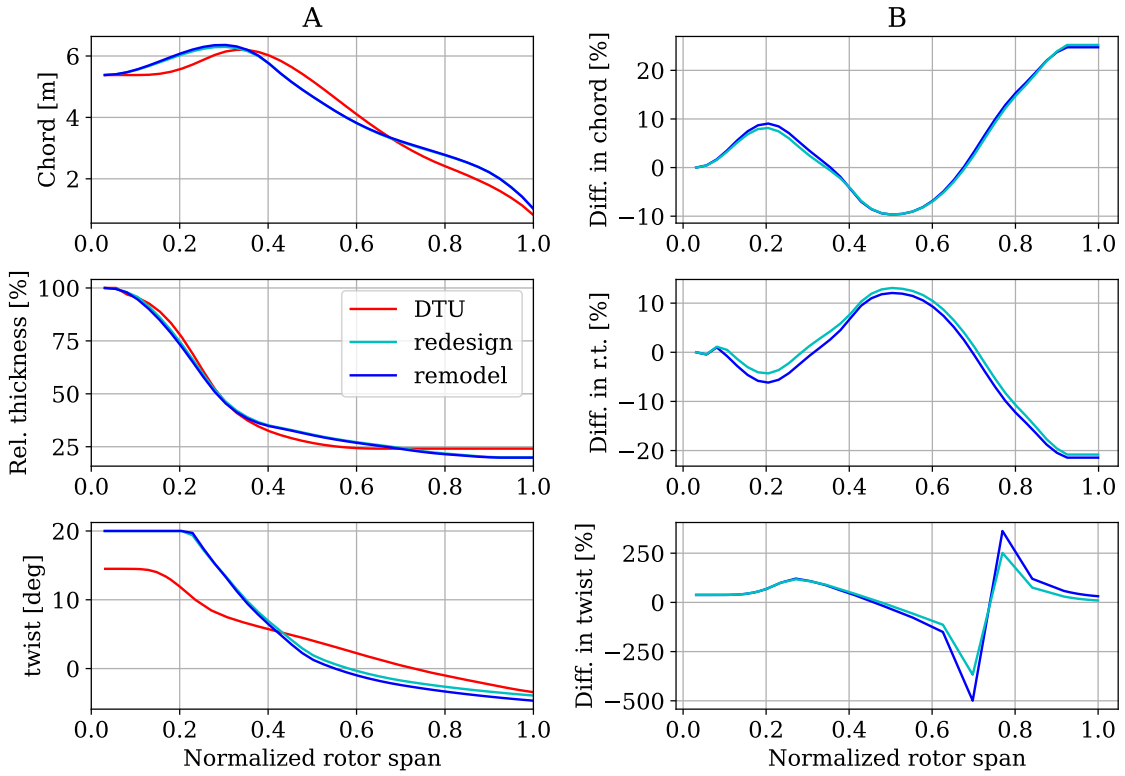

Figure 3: (A): chord, relative thickness and twist as a function of the normalized rotor span for the DTU 10 MW, the redesign and the remodel shape.
(B): percentual difference between redesign and DTU and remodel and DTU for chord, relative thickness and twist.

1.3 Blade performances

Having finalized the shape of the new blade, it is possible to test it using HAWC2S to evaluate the optimal TSR, as well as refine the blade performance characteristics previously computed with `single_point_design()`.
Firsly, HAWC2S is used to evaluate the blade at rated wind speed, resulting in Figure 4, comparing the performance of DTU 10 MW, the redesigned blade, and the remodeled blade. The effect of the new design function is visible in the C_l graph, which shows a larger lift coefficient compared to the redesign, which is even larger than the DTU's profile for normalized span larger than 0.4. For lower normalized span, the DTU blade uses Gurney flaps, that increase the performance. These addition is not applied in the redesign nor in the remodel.
Due to the increased twist near the root, the angle of attack can be reduced.
Also the induction factor a is effected by the different design choices. It is possible to compute the average value in the range [0.4, 0.9]: for the DTU 10 MW is 0.326, for the redesign is 0.312 and for the remodel is 0.380. Recalling that the induction is proportional to the quantity of wind subtracted by the turbine to the incoming wind, and its optimal value is 1/3, one can notice that the DTU 10 MW does quite a good job in achieving the optimal value, the redesign falls a little short and the remodel subtract more than necessary. Consequently, the production of the redesign was lower than expected, while for the remodel, this suggests that the power

production could increase. Unfortunately, this means that also the thrust force is larger, and larger loads are expected.
In fact, the C_P over the blade span for the remodel is larger than for the redesign, but so does the thrust coefficient. In these two plots one can really see the effect of the Gurney flaps in providing additional aerodynamic performance. Achieving the same results without this added feature is impossible based only on the `single_point_design()` function, so the discrepancy between remodel or redesign and DTU cannot be solved.

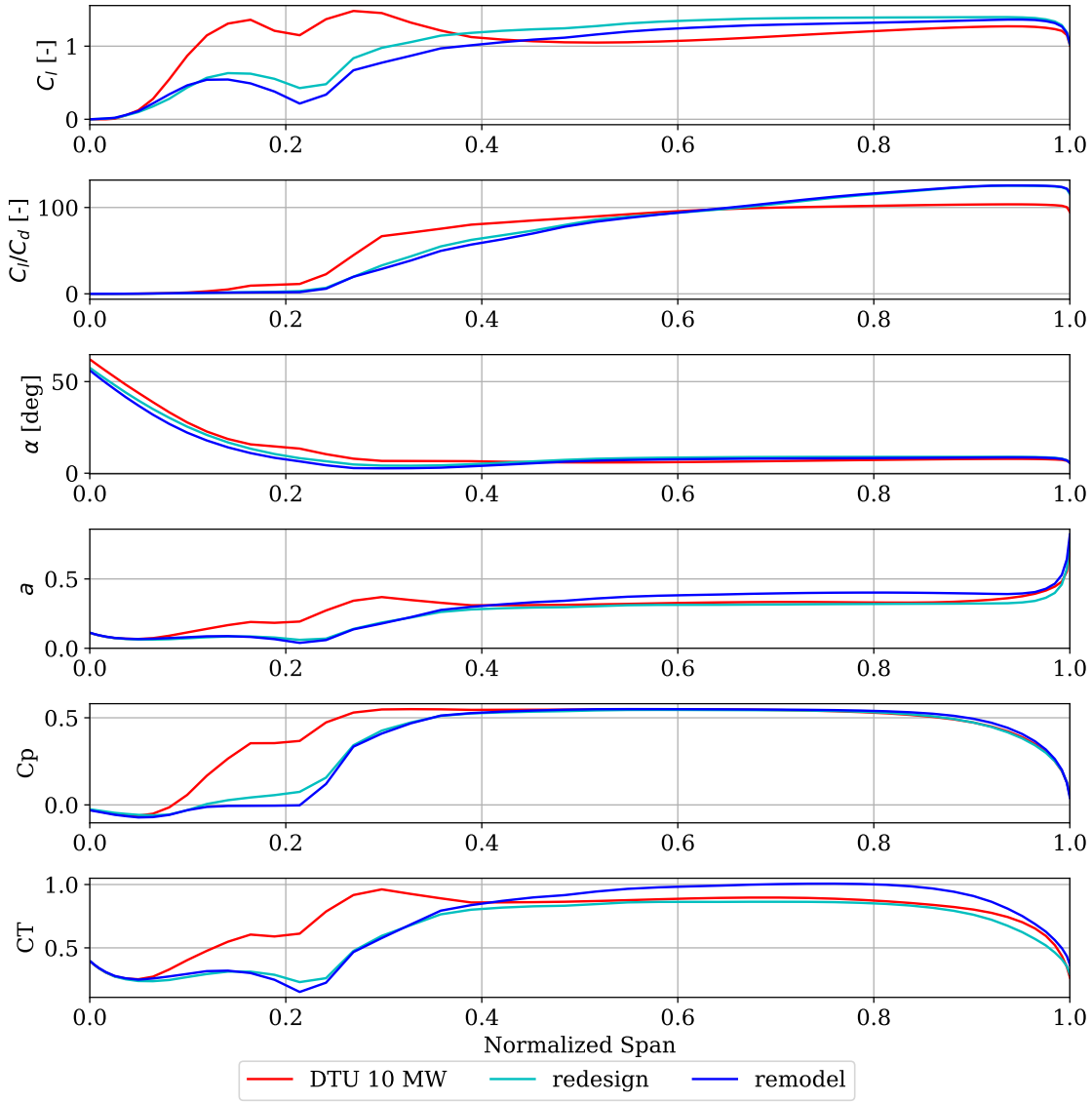

Figure 4: Lift coefficient Cl, lift over drag coefficient Cl/Cd, angle of attack α, induction factor a, power coefficient C_P and thrust coefficient C_T for DTU 10 MW, redesign and remodel blades.

The blade is then evaluated over a range of TSR to evaluate the optimal one. The resulting graphs can be seen in Figure 5. One can notice the increased accuracy of the HAWC2S software, which computes a different value of C_P for the same blade, if compared against the simplified BEM estimation of the `single_point_design()` function. Moreover, the remodel was able to

achieve the desired boost in performance, as the curve has higher values than the redesign's one.

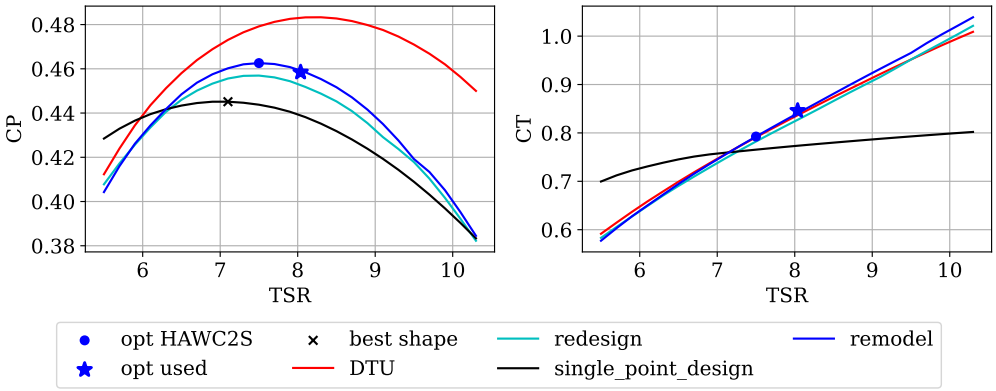

Figure 5: C_P and C_T curve over TSR for the `single_point_design()`, DTU 10 MW, redesign and remodel. 3 points are highlighted: 'best shape', meaning the ideal CP and TSR of the finalized blade shape evaluated using `single_point_design()`; 'opt HAWC2S', optimal values computed by HAWC2S for that specific blade; 'opt used', the final value found analytically.

Hence, the new maximum speed can be computed. As the power is constant after rated, and can be computed as torque times rotational speed, increasing the rotational speed will decrease the torque, hence the torque-related loads. The new value is based on the maximum allowed tip speed: to avoid velocity higher than 90 m/s on the tip, and having the radius fixed, the rotational speed cannot be increased more than 9.383 rpm, as computed by Equation 2. This value is similar to DTU maximum rotational speed, 9.6 rpm, and it quite larger than the redesign value, 8.337 rpm. To reach this value, the necessary TSR can be computed from Equation 3. This results in $TSR_{OPT} = 8.037$. Following the C_P over TSR curve previously described, one can find the correspondent $C_{Pmax} = 0.459$. It must be said that increasing the TSR does also increase the thrust coefficient, as highlithed in Figure 5.

$$\omega_{rated} = \frac{TS}{R_Y} * \frac{30}{\pi} \tag{2}$$

$$TSR = \frac{R_Y\, \omega_{rated}}{V_{ratedY}} * \frac{\pi}{30} \tag{3}$$

Lastly, the performance of the new blade can be evaluated for the operational wind speeds of the turbine using HAWC2S. A minimum rotational speed is implemented, to avoid resonance issues. This value is set as the DTU 10 MW minimum rotor speed, so 6 rpm. Note that if the minimum rotor speed is increased, also the pitch must be modified, to allow the turbine to still work in an optimal point in terms of TSR, pitch and relative C_P. Fortunately, the HAWC2S routine `compute_optimal_pitch_angle()` allows to optimize the pitch even at such low wind speed. Figure 6 displays the implemented minimum rotor speed, as well as showing the new rated rotational speed. Regarding the pitch, one can notice the increased value at low wind speeds. Moreover, at large wind speeds, DTU pitches less than the remodel, which is itself less

than the redesign. This can be related to the different dimensions of the 3 blades: the DTU's blade is the one with the smallest radius, so it is the one taking less energy from the wind. Hence, it does not need to pitch as much as the others to reduce its power output to the rated value. On the contrary, the larger redesign blade needs additional pitching to stay at rated power. As the remodel has a radius in between the two, so does the necessary pitching.

Moreover, the cut-in speed is reduced to 3 m/s. It can be recalled that the AEP is calculated on wind speed bins, centered around the wind speed and 1 m/s large, starting from 5 m/s. This means the first beam is 4.5 - 5.5 m/s, the second is 5.5 - 6.5 m/s and so on. Ideally, reducing the cut-in speed to 3 m/s should allow to fully encompass ad additional beam 3.5 - 4.5 m/s, hence increasing the computed AEP. Unfortunately, from Figure 7, one can notice that the power reaches negative value at such low wind speed. This means that there is not enough energy in the system at 3 m/s to allow such high rotational speed, so the power production is negative, meaning that the system needs additional energy to work. Of course, this is impracticable. Hence, having a minimum rotor speed and reducing the cut-in at the same time is impossible, and between the two, the minimum rotor speed is estimated to have a more beneficial impact for the turbine. In the following, the cut-in speed will be left at 4 m/s.

The last modification is applying the peak shaving. Essentially, the turbine starts pitching earlier, to reduce the thrust peak (hence the name). Consequently, the power is also reduced, but by a limited amount and only near rated. To implement this feature, the pitch needs to be manually changed and the resulting power and thrust are estimated, again using HAWC2S. As there is no defined rule to how to do it, a trial and error approach was used here, ultimately defining two peak shaving strategies: smallShave, that at rated has a pitch of 1 degree, and largeShave, that has a pitch of 2 degrees. SmallShave will be primarily used in the following evaluation and it is the one portrayed in Figures 6, 7 and 8, while the differences between smallShave and largeShave are displayed in Figure 9.

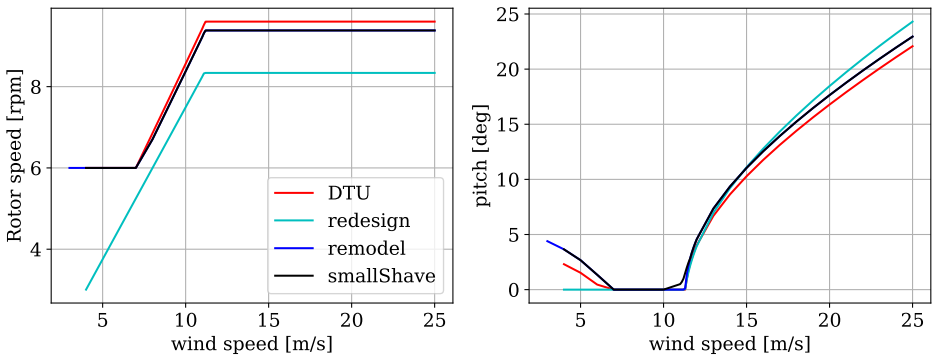

Figure 6: Rotor speed and pitch curve for DTU 10 MW, redesign, remodel and remodel with peak shaving.

At this point, it is still early to evaluate if the design challenge can be met. The power coefficient for the remodel in Figure 7 is higher than the redesign's one, so this suggests an improve in the performance, but it is still lower than the DTU 10 MW. Although, given the increased radius, the new design could still output more power. Regarding the thrust, the peak shaving appears an obligatory choice, as the remodel-without-peak-shaving profile has a larger thrust

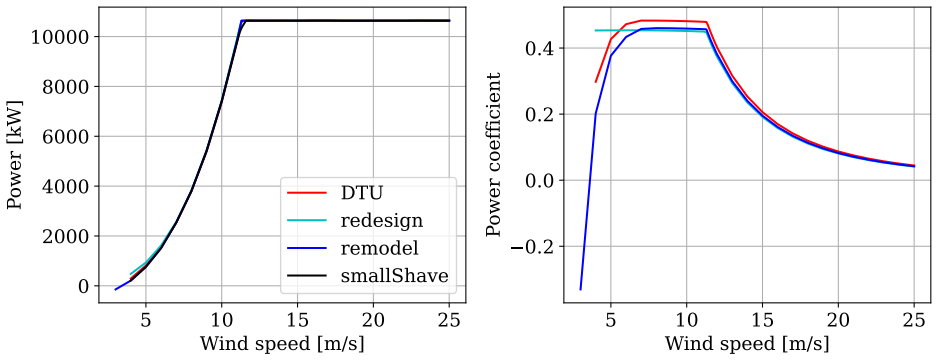

Figure 7: Power and power coefficient for DTU 10 MW, redesign, remodel and remodel with peak shaving.

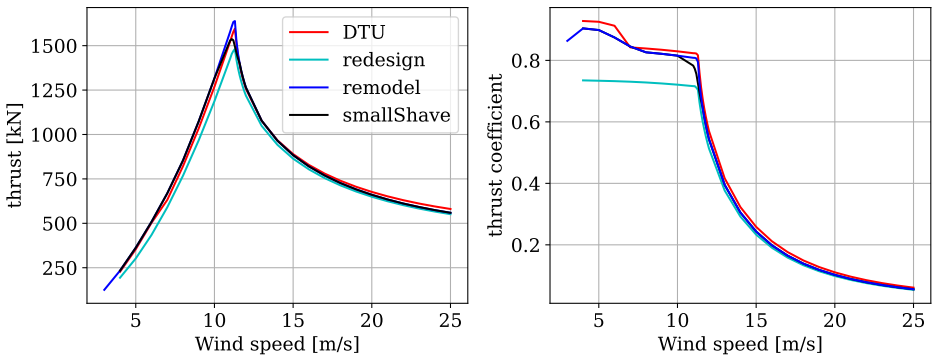

Figure 8: Thrsut and thrust coefficient for DTU 10 MW, redesign, remodel and remodel with peak shaving.

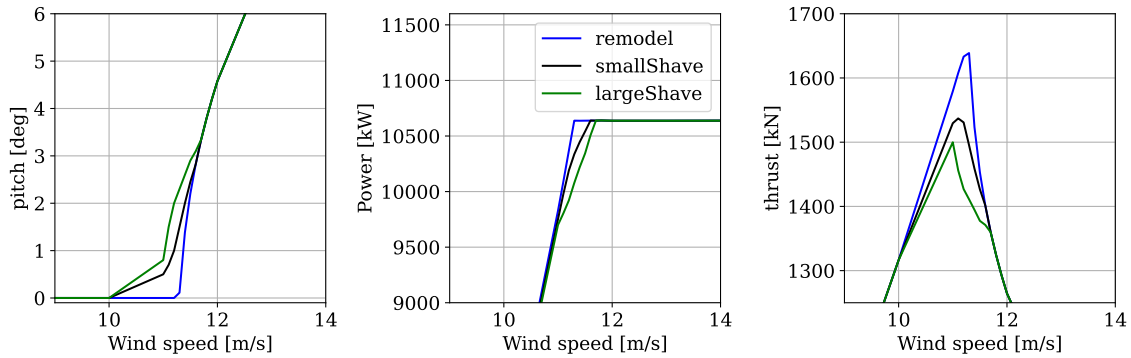

Figure 9: Pitch, power and thrust for the remodel, smallShave and largeShave.

than the DTU 10 MW, hence almost certainly higher loads. Regarding the thrust coefficient, the new design has a value significantly higher than the redesign, while fortunately being still lower than the DTU 10 MW. Additional analysis must be performed to assess the difference between the two shaving strategies.

2 Modal analysis

The aeroelastic modal analysis of the remodelled turbine can be performed using HAWCStab2 and aims to evaluate potential resonance issues. In particular, it seeks to answer the following question: Has the modified minimum rotor speed enabled the turbine to avoid resonance at a wind speed of 7 m/s?

A comprehensive analysis of the structural Cambell diagram is reported in the appendix. Essentially, the remodel behaves as expected, similar to the redesign and also similar to the original blade. One interasting thing is that the new blade has new natural frequency for the 1st flap and 1st edge, as reported in Table 3.

Table 3: Natural frequencies for the 1st flap and 1st edge frequency for the DTU 10 MW, the redesing and the remodel.

	1st flap [Hz]	1st edge [Hz]
DTU	0.5967	0.8904
redesign	0.6104	0.9306
remodel	0.5903	0.8823

Moreover, the aeroelastic Campbel diagram can be computed, again with HAWCStab2, and reported in Figure 10. In this type of diagram, the effect of the aerodynamic damping is portrayed. The natural frequencies previously defined are plotted as a function of the wind speed, together with the operational frequencies 1P, 3P and 6P. On the right, the corresponding modal damping is displayed. A resonance problem may occur when the operational frequency crosses a natural frequency, which is not or only lightly damped. Having modified the minimum rotor speed, hence the operational frequencies at low wind speed, there is only the crossing of the 6P with the 1st flap S and 1st flap FW, which are highly damped, and with the 1st edge BW, which is slightly damped.
Even though there is a crossing, it is unsure how much energy there is within the 6P frequency, and the 1st edge BW is still damped, even if only little. Moreover, looking at the aeroealstic Campel diagram for the DTU 10 MW in Figure 21, one can notice that a similar behaviour is present. It is unlikely that the remodelled turbine will encounter significant resonance problems, but a more solid Damage Equivalent Loads (DEL) analysis is needed to asses that.

Lastly, the components of each mode can be analyzed as a function of their amplitudes in Figure 22. In this graph, each row corresponds to a turbine modes, and it is displayed in terms of its degrees of freedom, each occupying a column. In the resulting boxes, the normalized amplitude of the degree of freedom is displayed. For the tower base FA, for example, the actual tower oscillation along the y direction is not the most significant component of the mode, as the FW flap, BW flap and S flap are present as well. On the other hand, for the tower base SS, the most significant component is actually the tower x oscillation. The other modes follows more or less what their name suggest, meaning that they have been correctly defined.

Recalling the question proposed above, adding a minimum rotor speed seems to have solved the resonance issues.

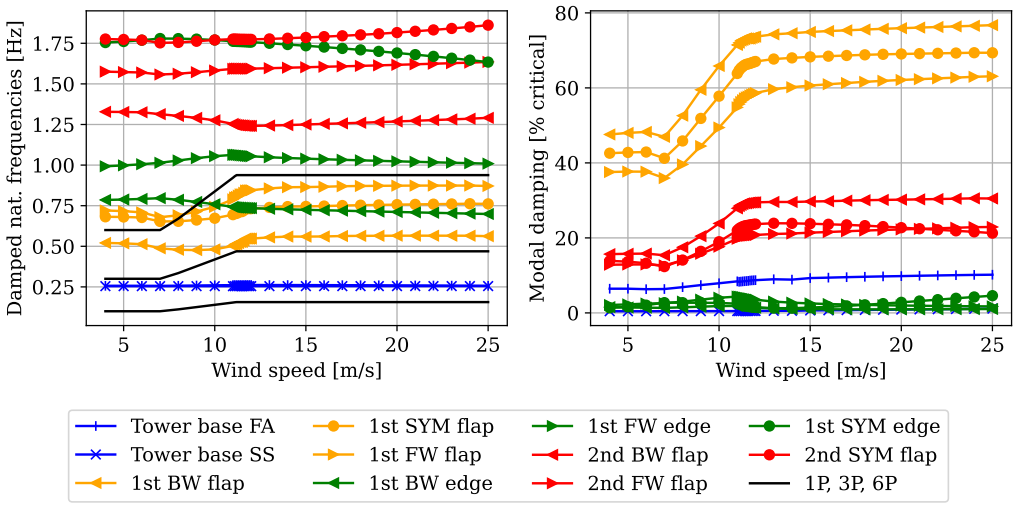

Figure 10: Aeroelastic Campbell diagram for the remodelled turbine

3 Control

Using HAWC2S and HAWC2 it is possible to tune the controller parameters, to obtain the best peformance out of the previously defined blade shape. To actually verify the controller efficiency, the turbine must be tested against real, turbulent wind: a task that is performed in the next section of this report. Here, the controller will be tested only against a pre-determined increasing wind, that is modified by a step function. Even though this is a simplified scenario, it still gives a good understanding on how the controller handles rapid increases in wind, and the response can be qualitatively defined in terms of the overshoot, so the difference between the maximum value reached and the reference value, and settling time, that is the time it takes the controller to stay at the reference value, +- a reasonable tolerance.

First of all, the turbine behaviour changes depending on the controller region. They are defined as follows:

1. **region 2:** Optimal C_P tracking, maximizes power output, first region, stops when the rotational speed reaches its maximum value
2. **region 2.5:** Speed-regulation, regulate rotor speed to a constant value, stops when power reaches it maximum
3. **region 3:** power and speed regulation, constant power region, either with constant torque or constant power strategy, final region

The boundary of these regions is portayed in Figure 11, with a zoom on region 2.5 in Figure 23 for the smallShave and largeShave input data. Due to the modified pitch behaviour, the two data have different regions boundaries. Likely, their behaviour will be different for incoming wind speed near V_{rated}.

Hence, a variety of controllers is tested to optimize the controlling strategy. Each controller is defined by an input natural frequency ω_Ω, a damping ratio ζ_Ω and a controller strategy, either

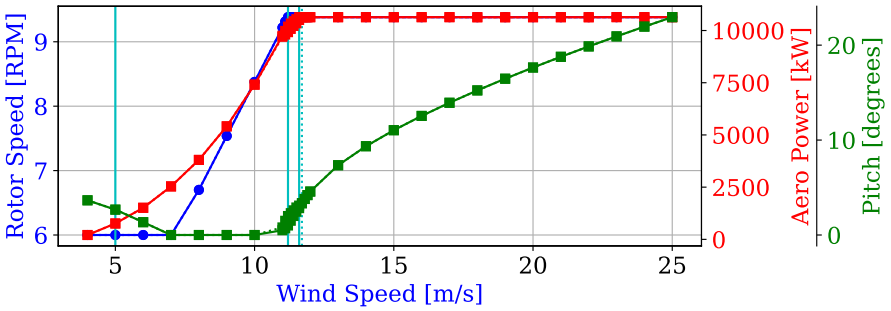

Figure 11: Rotor speed, power and region for the remodel with smallShave (full lines) and largeShave (dotted lines) and relative regions.

constant power or constant torque. From an intuitive prospective, ω_Ω is related to the settling time, meaning a higher natural frequency leads to a faster response, while the damping ratio acts on the overshoot, as increasing ζ_Ω reduces the overshoot error. Unfortunately, finding the 'perfect controller' is no easy task, as increasing ω_Ω or ζ_Ω too much may lead no instabilities, and each small adjustment must be tested, first with HAWC2S and then with HAWC2. Here, a total of 13 different controlling input was tested, starting from the controller C1 to C6 proposed in Assignemnt 3 [3]. From them, C1 resulted the most promising. Hence, 3 new controllers with different ω_Ω where tested and the optimal natural frequency, from controller C9, was kept in the following test series, that had new values for ζ_Ω. Finally, controller C12 was defined: this controller seems to outperform C1, but is unlikely the absolute best controller for this turbine. It is, however, a reasonable guess. The input parameters for the just defined controllers are reported in Table 4.

Table 4

	ω_Ω [Hz]	ζ_Ω [Hz]	constant power	Kp (rad/(rad/s))	Ki (rad/rad)
C1	0.05	0.7	yes	1.395	2.755
C9	0.04	0.7	yes	1.150	1.763
C12	0.04	0.6	yes	1.009	1.763

Then, the actual response of the turbine can be analyzed. The wind step applied to the controller can be seen in Figure 24, while the controller response is displayed in Figures 12 and 13 for controller C1 and C12 for both smallShave and largeShave, and controller C9 for smallShave. When comparing the smallShave controllers, the improvements from C1 to C9 to C12 can be easily seen, excpecilly in terms of settling time. The last controller is 'smoother' after the initial overshoot, and reaches the final value faster. The improvement is more noticible in the second step, around t = 470 s: altough the overshoot is larger for pitch and roational speed, the curves for the power, thrust and torque reaches the same maximum point but are faster in reaching the reference value. Conceptually, the controller acts on the pitch to control the loads, so it makes more sense to base our evaluation on the thrust and torque, not on the pitch itself.

Comparing the difference between smallShave and largeShave is more challenging. As one can see in Figure 12, largeShave has a lot of oscillations, with increased overshoot and settling time, expecially for the power. This behaviour can be seen only for the first step, as the differnce

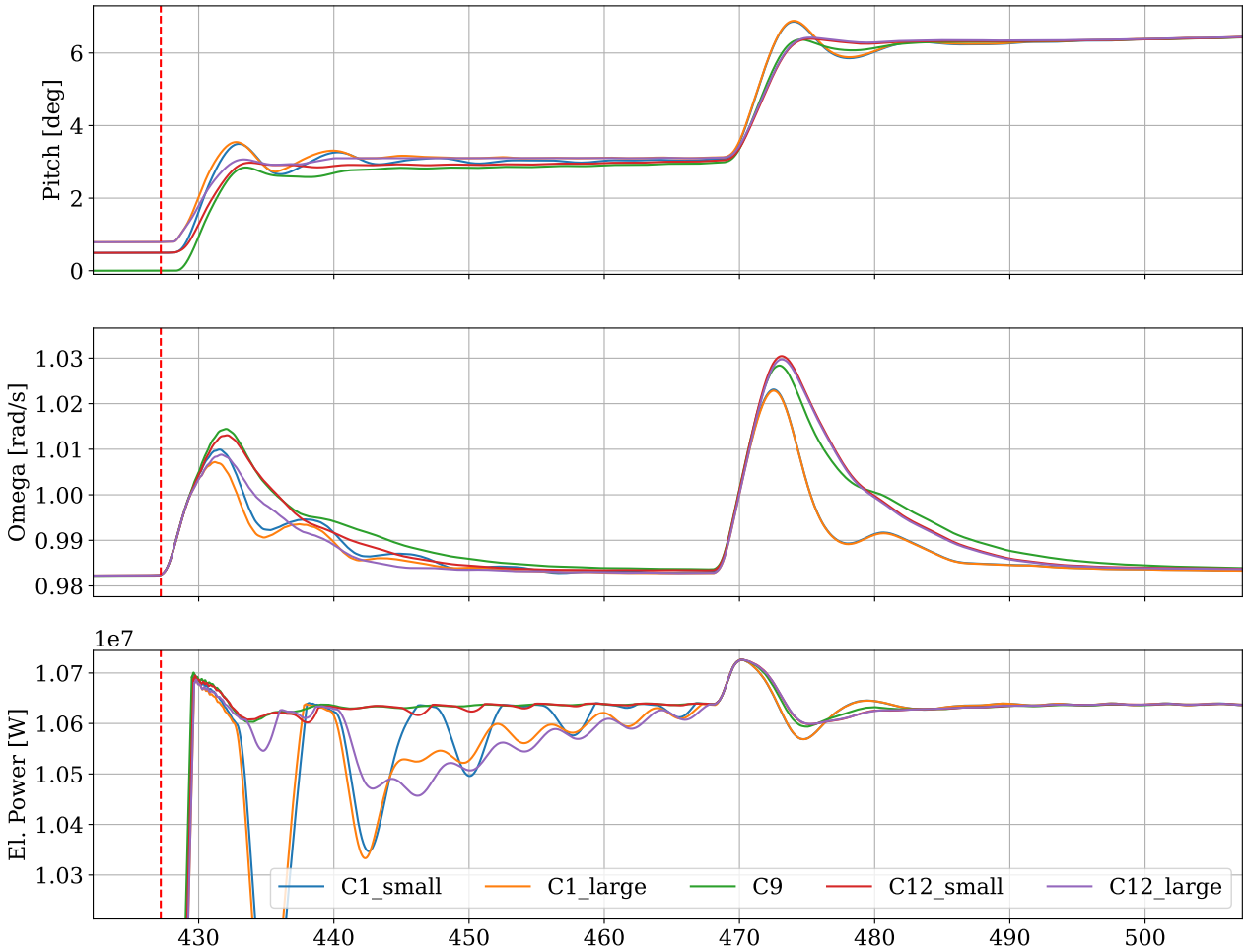

Figure 12: Pitch, rotational speed and electrical power for controller C1 and C12 for both smallShave and largeShave and C9 for smallShave. Vertical lines highlight the time where rated wind speed is reached.

between the two shaving strategies is only on a limited range of wind speed. Looking at this plot, one can be tempted to discard the largeShaving strategy. However, focusing on the thrust and torque graph, the overshoot for the frist step is actually reduced, suggesting that there could still be some potential in this stretegy. Hence, in the following, both controllers will be tested with turbulent incoming wind.

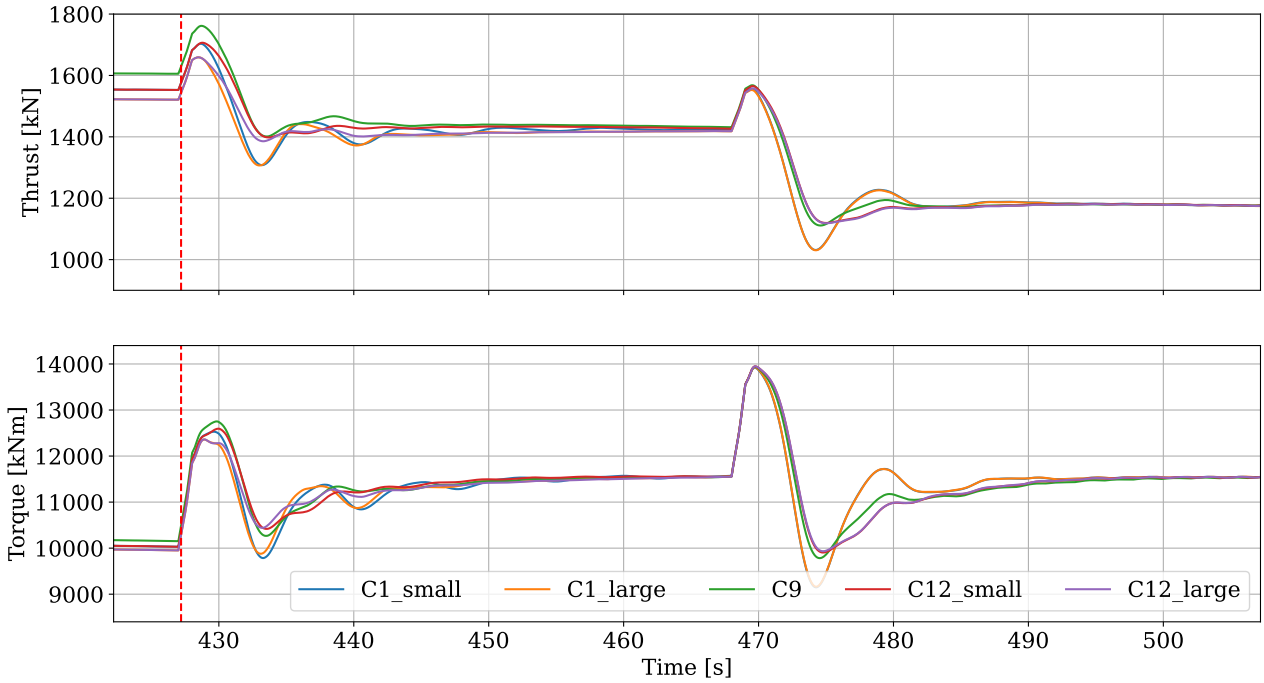

Figure 13: Thrsut and torque for controller C1 and C12 for both smallShave and large-Shave and C9 for smallShave. Vertical lines highlight the time where rated wind speed is reached.

4 Design loads

Finally, the turbine's behaviour against a turbulent wind is analyzed using HAWC2. For each wind speed, a 10-minute turbulent wind box with defined turbulence intensity is generated, and used to test the turbine. Six different realizations are performed per wind speed. Once all the simulations are run, the data can be fit together to find some useful insights: first of all, the operational data can be checked, to verify that the turbine behaves as expected. The rotor speed, pitch angle, generated torque, electrical power and thrust are plotted in Figure 25, for the DTU 10 MW, the redesign and the remodel. The resulting curves perform as anticipated. To achieve a higher AEP production, the simulations do not start from 5 m/s, as the DTU and the redesign, but at 4 m/s. Hence, one the graphs, the remodel has additional operating points at a lower wind speed. This and the following graphs portray the behaviour of controller C12 with the smallShave strategy.
One key difference between this graphs an the operational data proposed before is that the curves for torque and power do not reach the rated value at V_{rated}, but slightly after. Before rated, the controller efficiently reacts to the incoming turbulent wind, increasing the output power (same applies for torque) or decreasing it with the oscillating input. Hence, on average, it follows the previously defined curve. Near rated wind speed, however, the controller decreases with decreasing wind, but keeps the power at rated for increasing wind. Hence, on average, it outputs a value lower than the predefined. Only when the wind is so high that the turbulent wind is always higher than V_{rated}, the power is again at P_{rated}.
Looking again at the power curve, one can see that the 'constant power' controller strategy does not actually output a constant power, as the value is still oscillating, even if slightly. The

reason can be understood by looking at the mathematical implementation of the constant power strategy (Equation 4). As the controller actually filter the measured velocity with a Low Pass Filter (LPF), dividing the actual measured velocity by the filtered velocity returns an value oscillating around 1, hence the output power oscullated around rated.

$$\begin{aligned} \tau_{gen}(t) &= \frac{P_{rated}}{\Omega_{LPF}} \\ P(t) &= \tau_{gen}\,\Omega(t) = \frac{P_{rated}}{\Omega_{LPF}}\,\Omega(t) \end{aligned} \tag{4}$$

4.1 Extreme loads and fatigue loads

Moreover, the loads for different channels are computed. In general, the loads can be connected to two main sources of stresses on the turbine: thrust and torque. Additionally, gravity plays a role on some loads, even tough its effect is periodical, with a zero mean. The thrust loads tower base FA and out-of-plane blade root moment (BRM) are portrayed in Figure 14. Due to the increased thrust seen before, these loads are bigger (in magnitude) than DTU and than the redesign, expecially near rated.
The analyzed torque loads are tower base SS, shaft torsion and in-plane BRM, as one can seen in Figure 15. For the tower base SS, one can appreciate the absence of the resonance phenomenon at 7 m/s. This is the effect of adding the minimum rotational speed, and confirms the aeroelastic Campbell diagram proposed before. The shaft torsion reaches less extreme values than the redesign, altough it is still larger (in magnitude) than DTU. The in-plane BRM mean profile for the remodel is untouched, but the extreme values are hgher than DTU, even tough they are smaller than the redesign. The value of this load can be rougly computed following Equation 5. Hence, this is a gravity-related load. Is it clear now that the remodel places itself in between the other two turbines because so does its mass, that is essentially radius dependent.

$$M_{BR,y} = \frac{M_{\text{aero}}}{3} + M_{\text{self weight}}\cos(\psi) \tag{5}$$

From these loads, the extreme loads can be estracted. These are the average of the maximum loads (or minimum if it is larger in magnitude) multiplied by 1.35 to get the characteristic load, and then an additional 1.25 to compite the extreme loads. Their trends are proposed in Figure 27.

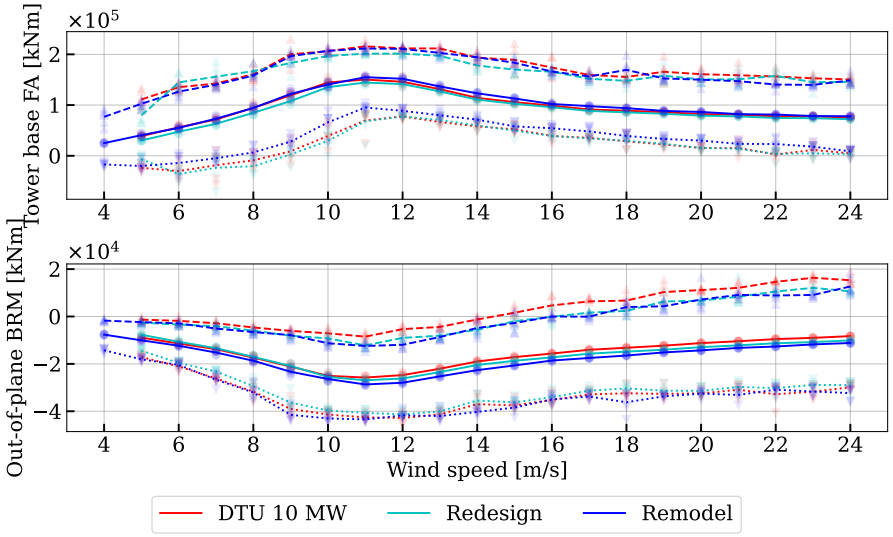

Figure 14: Thrust-related load computed by the turbulent simulations as a function of the wind speed. For each turbine 3 lines are proposed: max (–), mean (-) and min (..), and for each of them the actual simulated point are proposed as well.

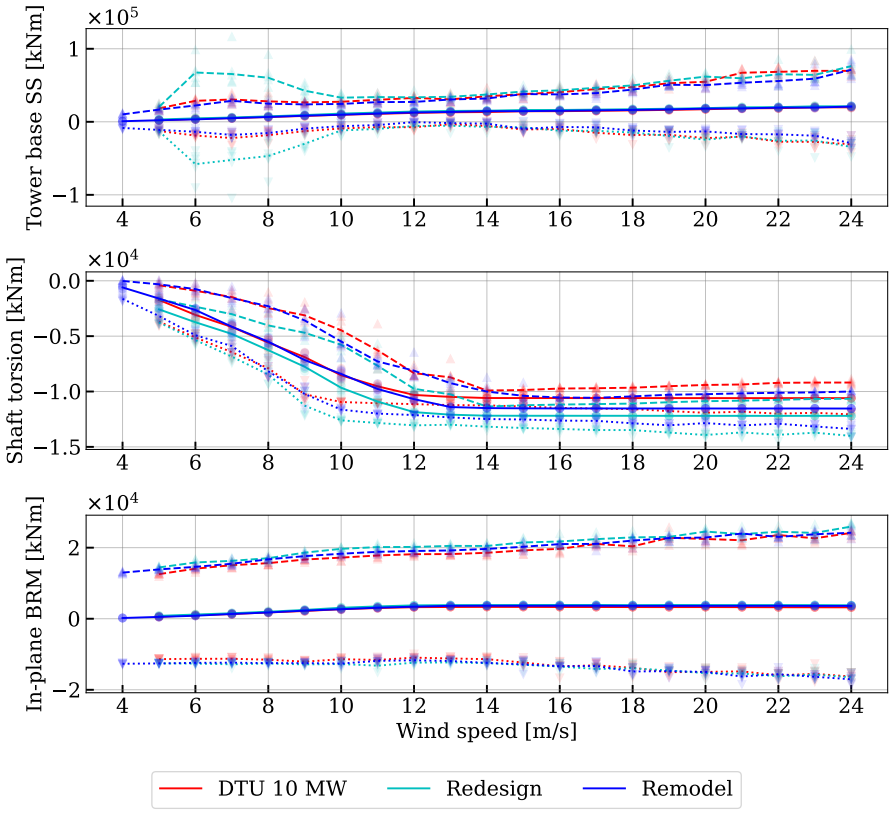

Figure 15: Torque-related load computed by the turbulent simulations as a function of the wind speed. For each turbine 3 lines are proposed: max (–), mean (-) and min (..), and for each of them the actual simulated point are proposed as well.

The postprocess operation performed on the turbulent simulations output computes the dam-

age equivalent load (DEL) for each channel, for each wind speed, and for each realization. The DEL is connected with the concept of fatigue: the larger and more frequent the oscillation of the loads previously described, the larger the fatigue stress on the turbine, hence the shorter its expected lifetime. The single DEL can be combined in an equivalent load R_{eq} knowing the Wohler exponent, which is material dependent. Hence, for a wind turbine, one can consider two main materials: the steel that is used for the tower and other hub components, and the composite material for the blade. Moreover, knowing the distribution of the wind between cut-it and cut-out, and the expected life of the turbine (20 years, normalized to 1e7 Hz), one can compute the lifetime equivalent load R_{eql}, which gives a realistic estimate of the expected loading throughout the lifetime of the turbine.
The 'steel' DEL are portrayed in Figure 16. Once again the absence of the resonance phenomenon positively effects the turbine response for the tower loads.
Figure 17 displayed the DEL for the 'composite channels'. Due to the increased load, the DEL increase as well, altough not as much as the redesign.

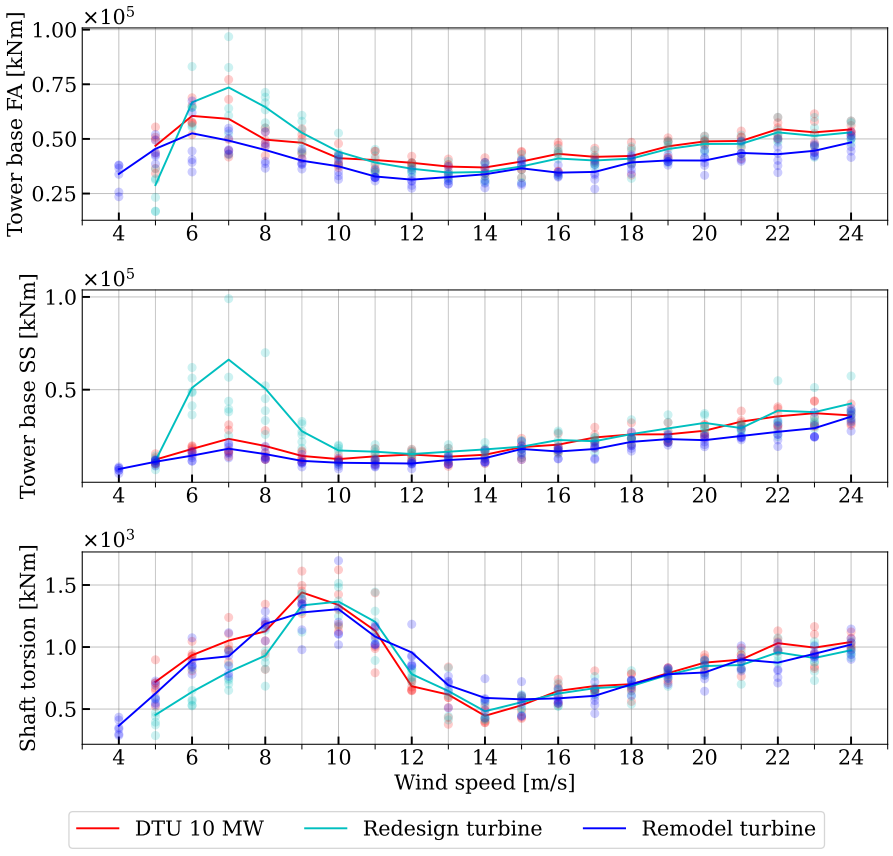

Figure 16: DEL and equivalent load for the loads that used the steel Wohler exponent = 4 for the DTU, remodel and redesign.

4.2 Tower clearance and AEP

An interesting channel to look at is the tower tip clearance, that is the minimum distance between the blade tip and the tower. During the blade design process, the blade has been

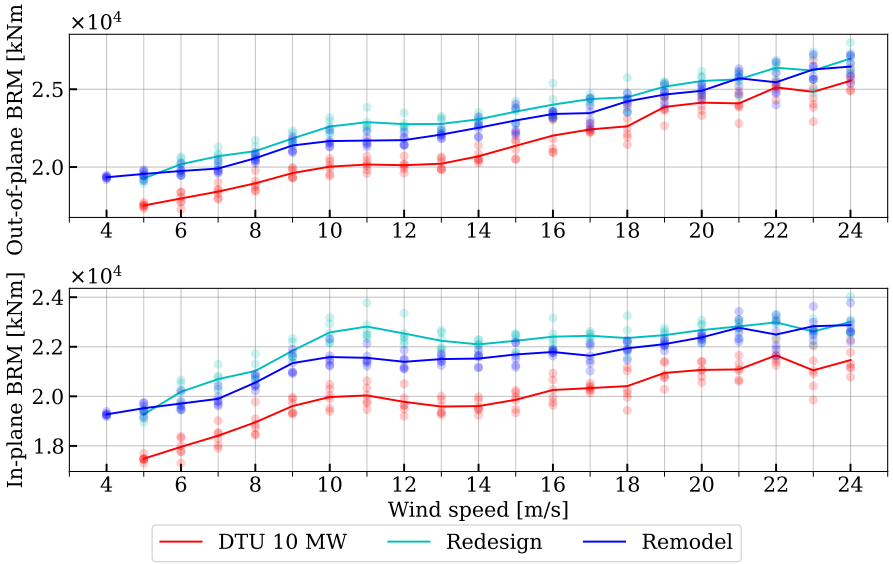

Figure 17: DEL and equivalent load for the loads that used the composite Wohler exponent = 10 for the DTU, remodel and redesign.

elongated, but the prebent has been kept constant. Moreover, the defined cone angle of 2.5 degrees has not been modified. This means that the blade tip was essentially brought further from the tower. Additionally, if one considers that the thicker blade deflects less, is it clear why the tower clearance has increased, as seen in Figure 26. The higher value of the tower clearance suggest a possible reduction of the cone angle to avoid eccessive loading due to unwanted gravity-related BRM.

The last thing that can be analyzed is the AEP. Following the IEC 61400-1:2019 standard, the wind speed distribution can be computed using the Rayleigh distribution, which is given by Equation 6. In the formula V_{ave} represents the reference wind speed for the wind class, as defined by Table 1. The operational range of the wind speed is devided in bins, as described above, and the production for each bin is calculated by computing the probability of the wind speed in each bin, multiplying it by the power production on that same bin (that is evaluated at the center of the bin), and multiplying it by the hours in an year, to have the annual production expressed in Wh. Finally, summing up the result for each bin gives the total annual production. Here the idea to decrease the cut-in speed, to add an additional bin (3.5 - 4.5) hence increasing the total production. Although the added bin is not fully contained in the cut-in to cut-out interval, the value of the power at its center (4 m/s) is known, so the AEP component for the added bin can be computed. As the cut-in cannot be lowered as described above, a simple solution is to halve the energy production for the added bin. In this way the computed production is actually between cut-in and cut-out, as it should. The energy production for each bin is portrayed in Figure 18

$$\begin{aligned} P(V_0) &= 1 - \exp\left[-\pi\left(\frac{V_0}{2V_{\text{ave}}}\right)\right] \\ P_{\text{bin}} &= P(V_1) - P(V_2) \end{aligned} \tag{6}$$

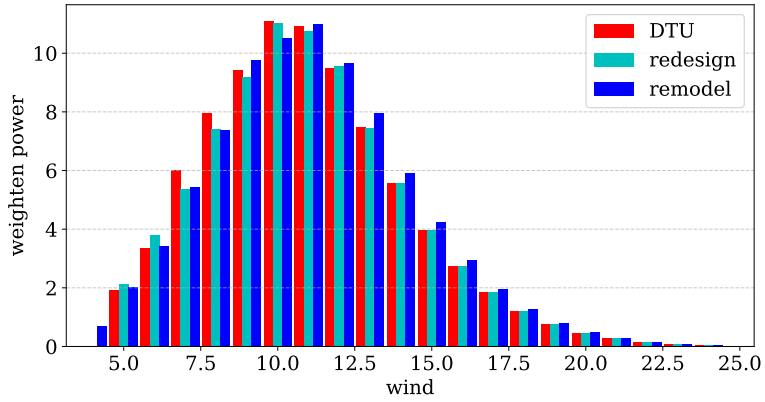

Figure 18: Energy production for each bin for the DTU, remodel and redesign.

One other thing to compare is the effect of the shaving intensity, smallShave and largeShave. To do so, the design loads, tower clearance, and production for the smallShave are compared with DTU values in Figure 19a, and for largeShave in Figure 19b. As one can notice, the increasing shaving does a significant job in reducing the loads, especially the equivalent lifetime loads. Unfortunately, also the power production decreases, as the percentual different with DTU 10 MW changes from +1.042% for the smallShave to +0.996% for the largeShave. Ultimately, the reduction on the loading added by the largeShave strategy makes it a superior strategy.
Finally, the choice of controller can be compared in a more informed way. Figure 19c shows the resulting loading condition for controller C1 with largeShaving applied, and its AEP is + 1.001% of DTU, making it more that the C12 largeShaving. Hence, C12 is not the optimal analyzed controller, but it was C1 all along. These data are also proposed numerically in Tables 5, 6, 7 and 8.

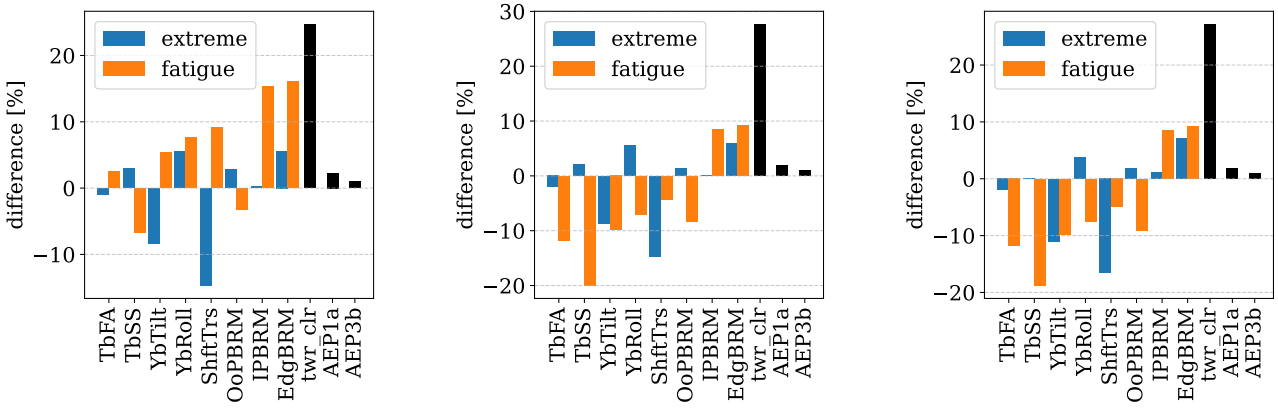

(a) C12 SmallShave **(b)** C12 LargeShave **(c)** C1 LargeShave

Figure 19: Percental difference between shaving and DTU for design loads and other significant parameters.

5 Conclusion

In this report, a new blade for the DTU 10 MW is designed and a thorough analysis of its performance is proposed. The first goal of the new design is to achieve a better result than Group 1's blade, and secondly to fulfill the design challenge: achieve higher AEP but similar or lower loads than the original blade for the new wind and turbulence class.
In particular, several design choices were modified from the redesign, and their effectiveness can be now evaluated. The shorter blade proved to be effective in reducing gravity loads, while still being large enough to have a sufficient energy intake. The changed chord did not provide identifiable changes. The reduced safety margin helped in increasing the lift along the blade, so it was a usefull addition. The increased rotor speed reduced the torque, altough it was still larger than DTU. An even higher rotor speed could have been used to increse this effect, altough achieving it requires a higher TSR, hence higher undesired thrust. The minimum lower speed proved to be extremely efficient in reducing the resonance issue found in the redesign. The peak shaving as well, expecially in its more aggressive implementation, provided a significant reduction in the design loads. Unfortunately, the cut-in speed was not lowered, but the AEP was still compute on a lerger interval, increasing its value.
Hence the question: did this blade fullfill the desing question? unfortunately only partially. For one, it has an higher production than the original DTU blade +1.001%, a result that was not obtained in the redesign. However, some loads are still higher than DTU 10 MW. These are gravity-related loads, and they are just going to be larger due to the larger blade.
Has it must be clear now, this design is not perfect, and some new changes could be done if a new blade was to be designed. First of all, the maximum chord can be increased, this time by a significant amount, to see what the effect would be. Additionally, new controllers can be tested, to verify if there is a better controller than C1. The peak shaving could be changed: since the AEP is higher than the DTU's production, one could 'trade' some excessive power for a reduction in loads, by increasing even more the peak shaving. Lastly, the chosen minimum rotor speed proved to solve the resonance issue related to the operational frequency hitting the tower resonance frequency, but it is still crossing the blade edge frequency. This phenomenon is not large enough to have a large impact on the loads, but it could still be quantified with a power density analysis.
In conclusion, the remodel outperformed the redesign in almost all metrics, but was still unable to fulfill the design challenge, although it came quite close.

Appendix

0.1 Part 2

Structural Cambell diagram

First, the structural Cambell diagram can be analyzed, as portrayed by Figure 20. Here, one can see the different frequencies of the various modes for changing rotational speeds. In particular, the tower has two possible modes: For-after FA, meaning the y direction (out of plane) and side to side SS, x direction, in plane. The blades can oscillate in the flap or edge direction, and for each of them there is a symmetrical whirling mode S, where all blades oscillate at the same time, and a backward whirling BW and forward whirling FW mode, where the synchronous behaviour is lost. At increasing rotational speed, the BW is reduced by a rate of $-\Omega$, while the FW is increased by a rate of $+\Omega$ [4]. Moreover, a phenomenon called rotational stiffening accours: the rotating body increases its stiffening, hence the symmetrical mode is not perfectly horizontal but increases at increasing omega. To find the theoretical curves, one can evaluate the natural frequency of the single body (tower and blades), and this value should match the turbine frequencies at 0 rpm. Table 20 reports the natural frequency of the blade. It can be noticed that the 3 blades have different natural frequencies, and they are not in a 'radius size order'. These frequencies depend on how the mass is distributed along the blade length, so they depends on all the blade parameters. Additionally, having a larger or lower frequency is not a good or bad thing on its own, it depends on the operational regime of the system [1]
The 1st edge symmetrical is referred as drivetrain mode because it changes consistently from the theoretical behaviour previously defined. This is due to the boundary conditions being modified, from fixed-free to pinned-free, and this changes the structural response of the system. As a blade is essentially a cantilever beam, it experiences several modes: here the 1st is portrayed, characterized by 1 node where the cantilever body is attached, but there are also 2nd modes, with 2 nodes, and higher.
Finally, the difference between the theoretical curves and the actual curves in the figure can also be related to the presence of the tower, that has some level of flexibility, hence some influence on the other modes.

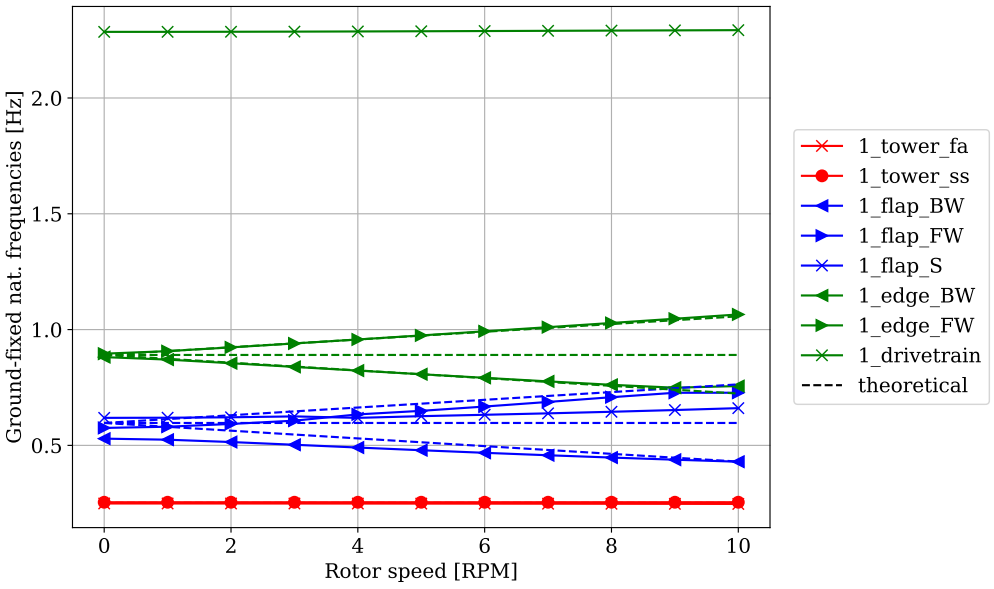

Figure 20: Structural Campbell diagram for the remodelled turbine

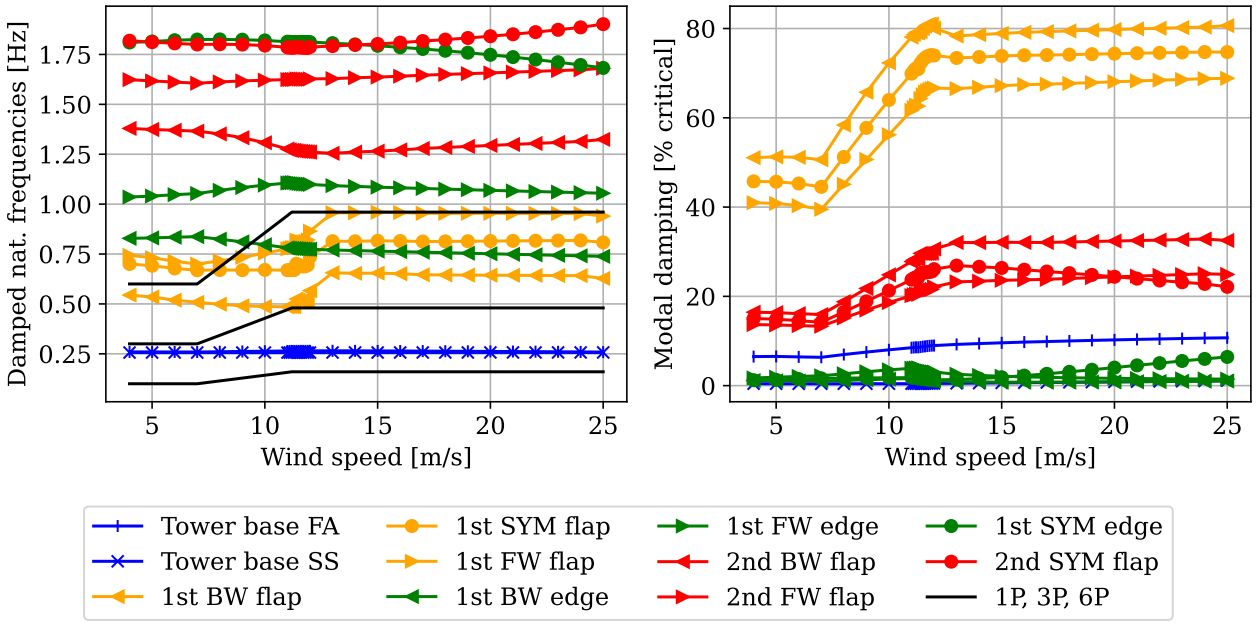

Figure 21: Aeroelastic Campbell diagram for the DTU 10 MW turine.

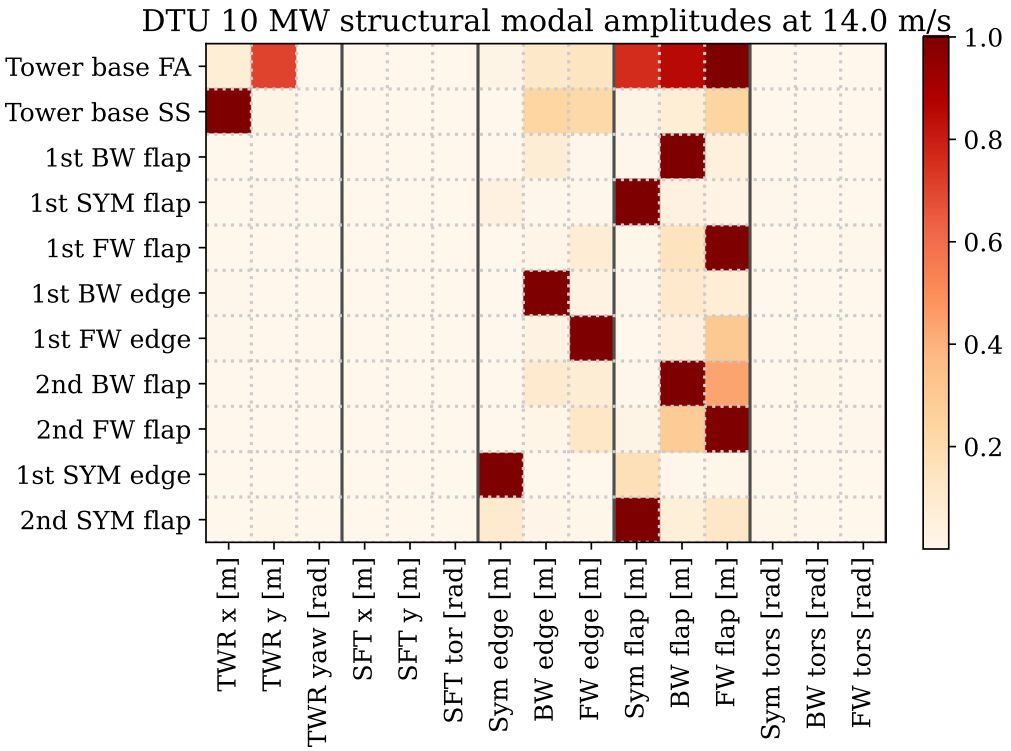

Figure 22: Amplitude of the analyed vibrational modes. The given name is on the left and the degree of fredom on the bottom.

0.2 Part 3

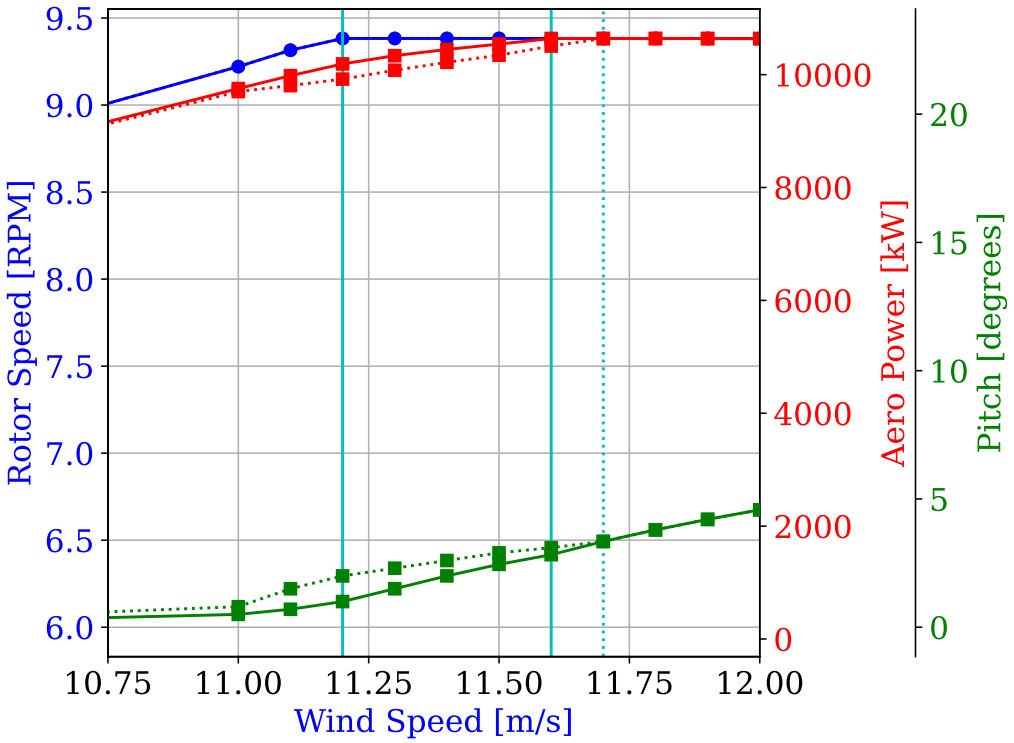

Figure 23: Rotor speed, power and region for the remodel with smallShave (fulle lines) and largeShave (dotted lines) and relative regions, zoom on region 2.5

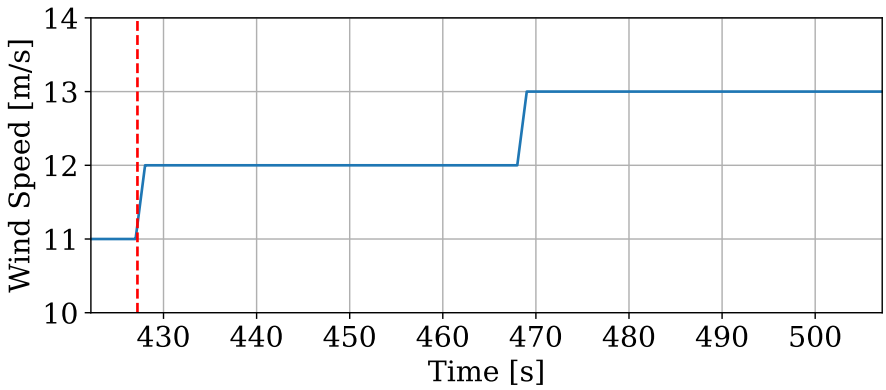

Figure 24: Step wind applied to the controller. Vertical lines highlight the time where rated wind speed is reached

0.3 Part 4

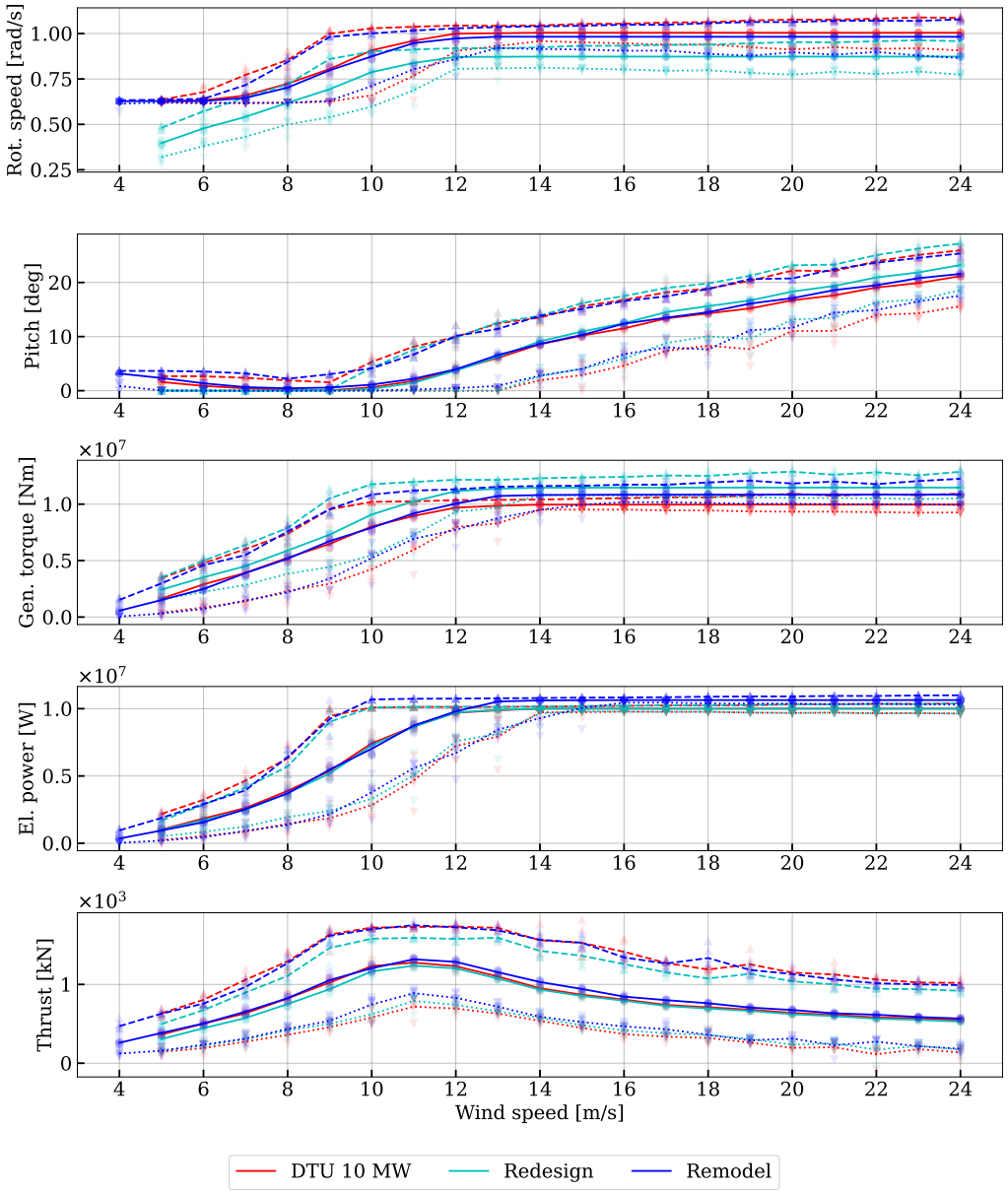

Figure 25: Rotor speed, pitch angle, generated torque, electrical power and thrust for DTU 10 MW, redesing and remodel computed by the turbulent simulations. For each turbine 3 lines are proposed: max (–), mean (-) and min (..), and for each of them the actual simulated point are proposed as well.

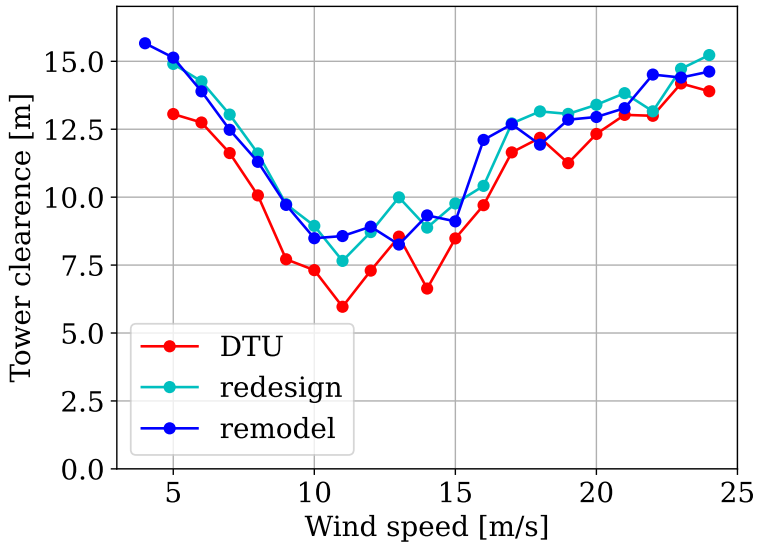

Figure 26: Tower clearance as a funcion of the wind speed for DTU 10 MW, redesign and remodel.

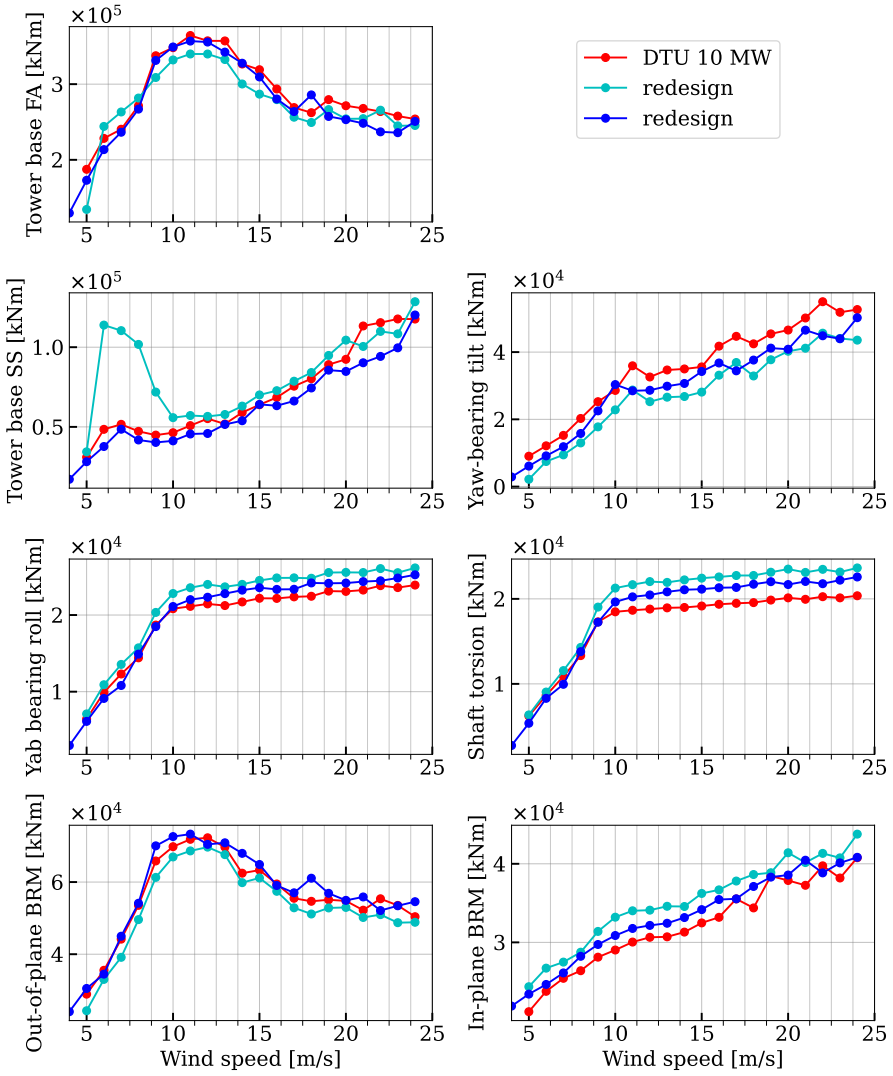

Figure 27: Extreme loads as a function of the wind speed for the analyzed channels. The actual extreme load value is the maximum of the proposed plot

0.4 Summary values

Channel	Extreme Load [kNm]	Extreme Load (%)	R_{eql} [kNm]	R_{eql} [kNm] %
TbFA	360956.900	-0.917	134997.456	2.453
TbSS	121233.693	2.985	44905.083	-6.773
YbTilt	50357.086	-8.421	28710.890	5.316
YbRoll	25235.445	5.555	4089.134	7.640
ShftTrs	22590.859	-14.670	3123.355	9.161
OoPBRM	74264.432	2.752	27169.096	-3.229
IPBRM	40857.820	0.214	33411.594	15.302
EdgBRM	30603.483	5.611	32792.922	16.122

Table 5: C12 smallShave: Extreme load and fatigue metrics with percentage differences.

Channel	**Extreme Load [kNm]**	**Extreme Load (%)**	R_{eql} **[kNm]**	R_{eql} **(%)**
TbFA	356920.062	-2.025	116150.990	-11.850
TbSS	120221.129	2.124	38546.994	-19.973
YbTilt	50229.850	-8.653	24574.291	-9.857
YbRoll	25247.807	5.606	3533.095	-6.997
ShftTrs	22574.232	-14.733	2736.333	-4.365
OoPBRM	73286.781	1.400	25742.034	-8.312
IPBRM	40822.870	0.128	31436.639	8.487
EdgBRM	30679.463	5.873	30833.925	9.185

Table 6: C12 largeShave: Extreme load and fatigue metrics with percentage differences.

Channel	**Extreme Load [kNm]**	**Extreme Load (%)**	R_{eql} **[kNm]**	R_{eql} **(%)**
TbFA	356978.698	-2.009	116181.133	-11.827
TbSS	117775.795	0.047	39132.305	-18.758
YbTilt	48914.809	-11.044	24592.649	-9.790
YbRoll	24813.638	3.790	3512.578	-7.537
ShftTrs	22089.388	-16.564	2718.475	-4.989
OoPBRM	73631.265	1.876	25527.504	-9.076
IPBRM	41257.836	1.195	31425.123	8.447
EdgBRM	31057.876	7.179	30826.648	9.159

Table 7: C1 largeShave: Extreme load and fatigue metrics with percentage differences.

Configuration	**AEP [GWh]**	**1a (%)**	**3b [GWh]**	**3b (%)**
C12 smallShave	50.385	2.267	34.300	1.042
C12 largeShave	50.220	1.932	34.285	0.996
C1 largeShave	50.220	1.933	34.287	1.002

Table 8: AEP and relative differences for 1a and 3b configurations.

Bibliography

[1] Celik Ahmet. "Wind Turbine Blade Flapwise and Edgewise Bending Vibration Analyses Using Energy Methods". In: *Journal of Thermal Engineering* 2 (Oct. 2016). DOI: 10.18186/jte.96366.

[2] Christian Bak and Kenneth Lønbæk. "Aerodynamic Rotor Design Loads, aerodynamics and control of wind turbines Design of the 10MW rotor". In: (2024).

[3] Nicola Quaia, Mathéo Chalas, and Bogusz Adam Glaza. *Controller Tuning*. Nov. 2024.

[4] Riccardo Riva. "Campbell diagram". In: (2024). URL: https://wtstab.pages.windenergy.dtu.dk/stability-analysis-of-wind-turbines/campbell_diagram.html.